ACS APPLIED MATERIALS & INTERFACES

Research Article

www.acsami.org

Wide Range Photodetector Based on Catalyst Free Grown Indium Selenide Microwires

Zulfiqar Ali,[†] Misbah Mirza,[‡] Chuanbao Cao,*[,†] Faheem K. Butt,[†] M. Tanveer,[†] Muhammad Tahir,[†] Imran Aslam,[†] Faryal Idrees,[†] and Muhammad Safdar[‡]

[†]Research Centre of Materials Science, School of Materials Science and Engineering, Beijing Institute of Technology, Beijing100081, People's Republic of China

[‡]National Center for Nanoscience and Technology, Chinese Academy of Sciences, Beijing 100190, People's Republic of China

ABSTRACT: We first report the catalyst free growth of indium selenide microwires through a facile approach in a horizontal tube furnace using indium and selenium elemental powders as precursors. The synthesized microwires are γ-phase, high quality, single crystalline and grown along the [11$\bar{2}$0] direction. The wires have a uniform diameter of ~1 μm and lengths of several micrometers. Photodetectors fabricated from synthesized microwires show reliable and stable photoresponse exhibiting a photoresponsivity of 0.54 A/W, external quantum efficiency of 1.23 at 633 nm with 4 V bias. The photodetector has a reasonable response time of 0.11 s and specific detectivity of 3.94×10^{10} Jones at 633 nm with a light detection range from 350 to 1050 nm, covering the UV−vis-NIR region. The photoresponse shown by single wire is attributed to direct band gap (E_g = 1.3 eV) and superior single crystalline quality. The photoresponsive studies of single microwires clearly suggest the use of this new and facile growth technique without using catalysts for fabrication of indium selenide microwires in next-generation sensors and detectors for commercial and military applications.

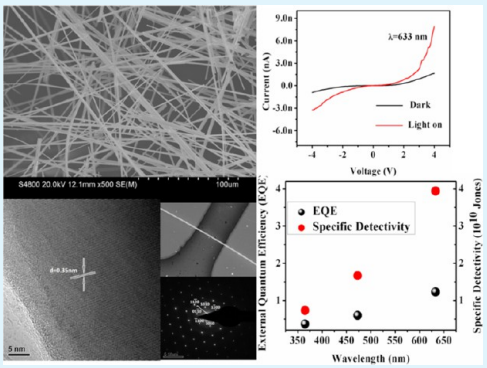

KEYWORDS: *indium selenide, catalyst free growth, microwires, photodetector, semiconductor*

INTRODUCTION

One-dimensional (1D) crystal structures are important for optoelectronics and future nanoscale devices as they allow interconnections within their size limits.[1−9] There are reports on nanoscale device fabrication and these devices have shown significant progress in building a new generation of electronic and photoelectronic systems.[10−14] Photodetectors are necessary devices in memory storage and optoelectronic circuits and various semiconducting materials like group III-V compounds and group II-VI compounds[15−17] have been used in fabricating photodetectors but are limited due to poor efficiency.

Indium selenide (In_2Se_3) is an important narrow band gap III-V semiconducting material with a layered crystal structure. It usually crystallizes into double layers consisting of the [Se−In−Se−In-Se] stacked together through Se atoms along the *c*-axis.[18] Highly anisotropic structural, electrical, optical and mechanical characteristics of this material[19] make the phase attractive for photovoltaic solar cells, ionic batteries, optoelectronic and phase change memory devices.[20−25] However, most of the work is reported on indium selenide thin films;[26−29] only a limited number of reports focus on 1D growth of indium selenide nanostructures and its potential properties for applications in electronic, optoelectronic, phase change memory and thermoelectric devices. All such reports accentuate on the catalyst assisted growth of wires or rods through a VLS growth mechanism,[30−34] thus obtaining the α-phase of this material. There is only one report on catalyst free growth of indium selenide[35] using In_2Se_3 as a precursor but the phase reported is InSe in 1:1 stoichiometric ratios. The reason for no such reports has been the difficulty in controlling the chemical reaction and morphology at the same time.

On the other hand, using a catalyst (usually Au) for 1D nanostructures not only makes the growth expensive but also Au particles are incorporated in the crystal during the growth, thus adding impurity in the crystal structure. The photoresponse exhibited by such structures cannot be considered purely due to indium selenide.

We report here for the first time, the growth of pure phase γ-In_2Se_3 without utilizing any catalyst; we not only control the chemical reaction but also obtain high yield, ultralong and high quality indium selenide (In_2Se_3) microwires using elemental indium and selenium powders as precursors through a vapor−solid (VS) approach. Furthermore, single microwire In_2Se_3 photodetectors are fabricated and photoresponse characteristics were schematically examined under a broad light range from 350 to 1050 nm. The photodetector shows appreciable performance in this broad wavelength range. The results suggest that catalyst free growth of In_2Se_3 in a 1D structure with controlling diameters will open a gateway toward the

Received: March 30, 2014
Accepted: May 17, 2014
Published: May 17, 2014

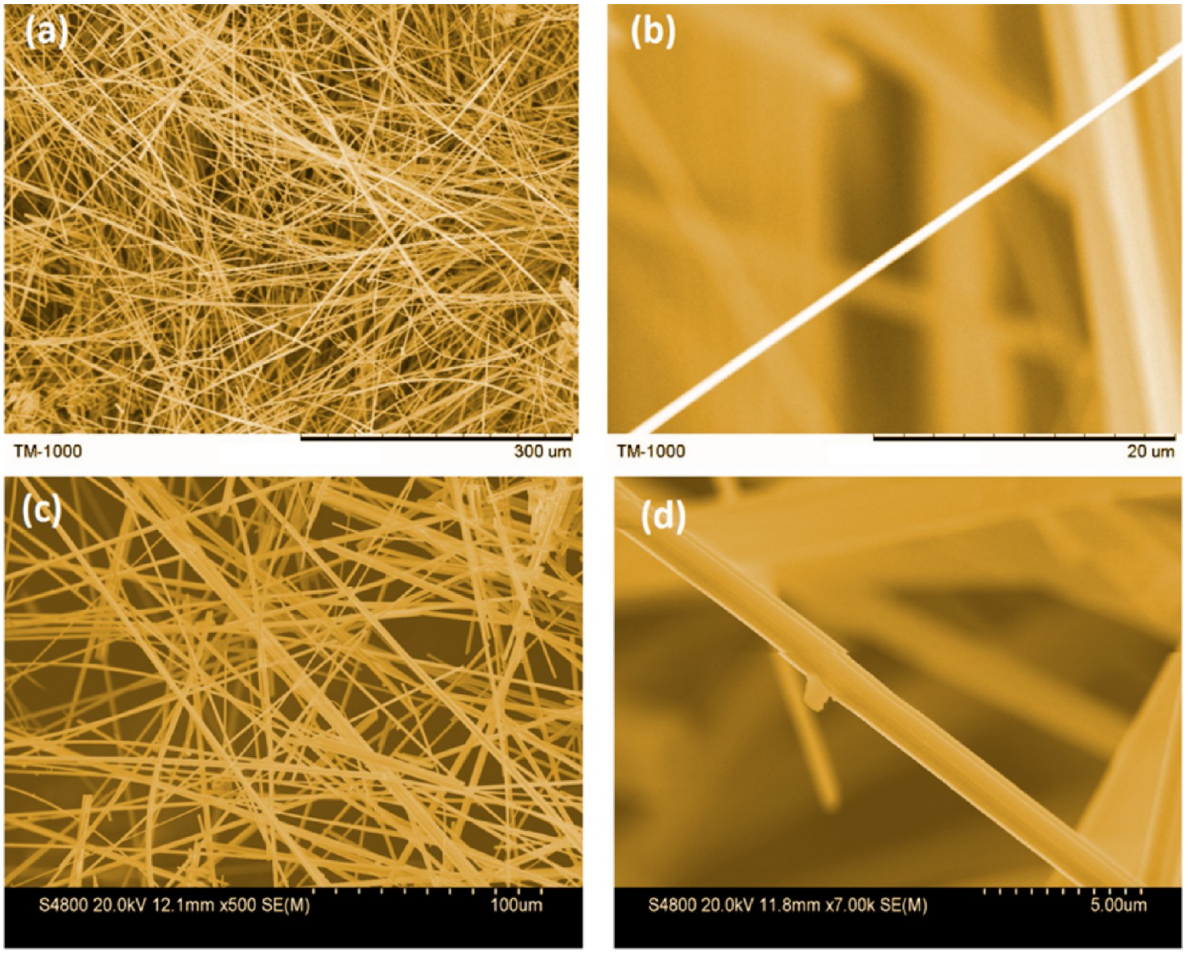

Figure 1. (a) SEM micrographs at 300 μm scale showing large scale production of In_2Se_3 microwires using VS synthesis technique. (b) SEM micrograph of a single microwire at 20 μm scale. (c) FESEM micrographs acquires at 100 μm scale to observe the morphology. (d) High resolution FESEM image to estimate the diameter of single microwire.

nanodevice fabrication and research on photodetectors of this material.

EXPERIMENTAL SECTION

A mixture of indium (In) and selenium (Se) powders (99.99%) in 2:3 mol ratios was placed in a quartz crucible to prepare single crystalline high quality indium selenide microwires. The quartz crucible was sealed air tight and further wrapped with aluminum foil to preserve the inert environment for the system. This crucible was placed in the center of a horizontal tube furnace with a 50 mm inner diameter. The furnace tube was first evacuated using a mechanical rotary pump and purged heavily with high purity Ar gas for 3 h in order to eliminate any oxygen contents in the tube. The flow rate and pressure in the furnace tube were kept 60 sccm and 200 Torr, respectively. The system was heated gradually at the rate of 2 °C/min to reach a target temperature of 700 °C and kept at this temperature for 24 h. Then it was cooled down to room temperature naturally.

Characterizations. The synthesized products were characterized by field emission scanning electron microscopy (FESEM, Hitachi S-4800) and high resolution transmission electron microscopy (HRTEM, FEI F20) with X-ray energy dispersive spectrometry (EDS). The structure and phase purity was tested by X-ray powder diffraction (XRD, Philips X'Pert Pro MPD) with Cu Kα radiation (λ = 0.154 06 nm).

Fabrication of Single In_2Se_3 Microwire Device and Its I–V Measurements. The In_2Se_3 microwires were dispersed in ethanol by sonification and drops were casted on silicon wafers with a 300 nm thick thermal oxide layer. The electrical contacts to individual In_2Se_3 microwire were defined by a copper grid shadow mask with the typical gaps of 15 or 20 μm, and subsequently 8 nm Cr and 100 nm Au was evaporated, respectively. The transport characteristics of these devices were measured at room temperature in the ambient air using an ever being manual probe station equipped with a Keithley 4200 semiconductor characterization system. To initiate the photocurrent, we measured DC photoconductivity at room temperature in ambient air by illuminating the devices using a relative light source.

RESULTS AND DISCUSSIONS

Morphology of the products was initially examined by SEM, high resolution micrographs of the product are presented in Figure 1a, which depicts the large scale growth and ultralong (~ centimeter) range, even in the 30 μm scale, all the area is covered with microwires. Figure 1b shows the single microwire, and the diameter estimated with SEM was about 1 μm. Microwires were further examined morphologically with the help of FESEM and the large scale growth and the diameter were confirmed to be ~1 um, as shown in Figure 1c,d. It is clear from the FESEM images that the surface of microwires is smooth and uniform diameter all along its length.

Figure 2 shows the morphology of the product at the base of the powders, which is really useful in understanding the growth mechanism of the wires. Figure 2a–d represents micrographs taken at different areas at the bottom of powders, because the product obtained was in the shape of a solid with microwires grown on the top and the base was kind of a hard solid. This

dx.doi.org/10.1021/am501933p | ACS Appl. Mater. Interfaces 2014, 6, 9550–9556

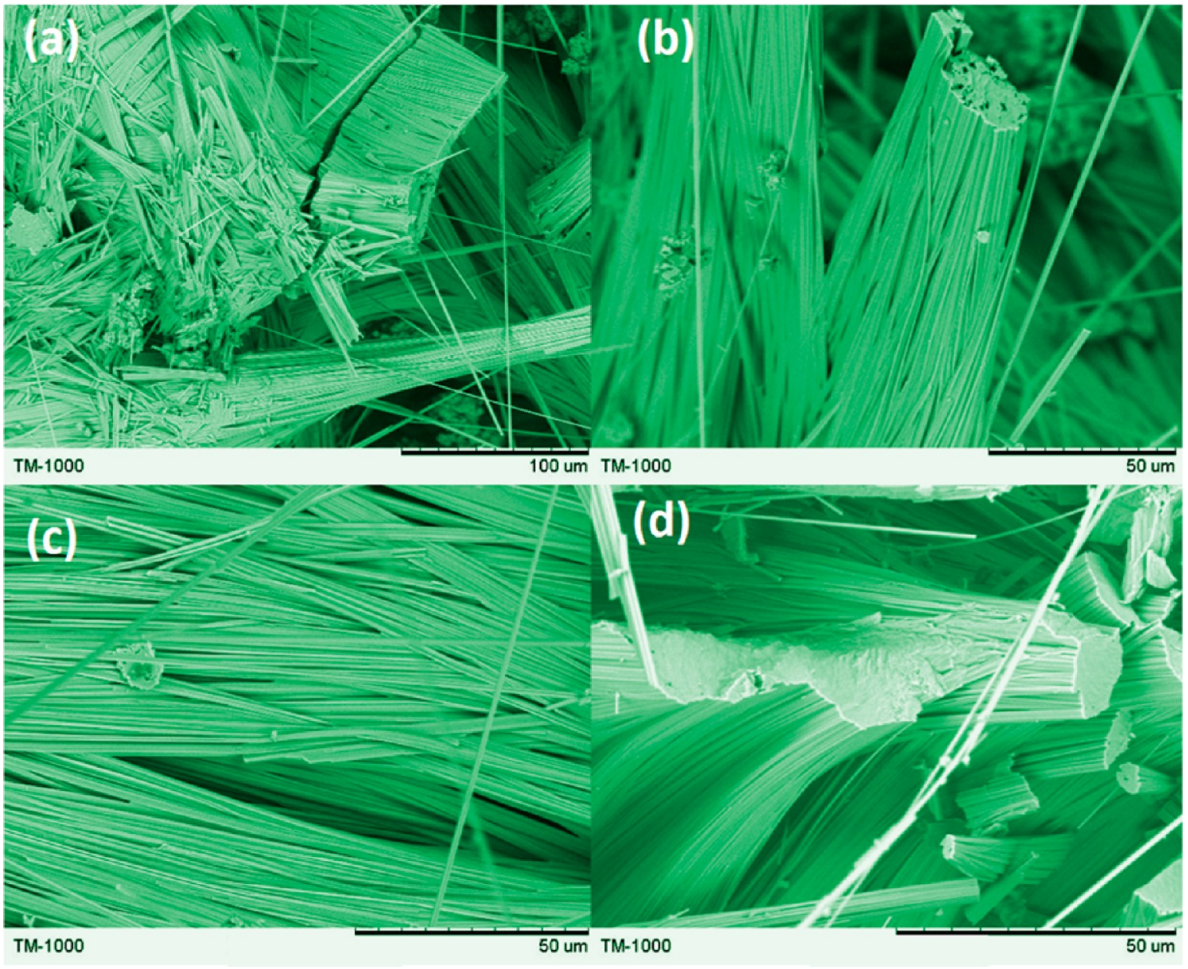

Figure 2. (a) SEM micrographs of the product at base showing large scale production in the form of bundles. (b) High resolution micrograph of bundles. (c) SEM micrographs of bundles from the middle showing ultralong microwires. (d) Different view of bundle formation.

figure clearly suggests that at the start, the mixture of powders first solidifies in the shape of bundles and chemical reaction takes place at this stage. As the internal energy of the system increases because the product was placed at 700 °C for 24 h, these solid bundles break up into 1D structures. At the final stage, these wires grow longer on the upper portion and breakup from the solid bundles. Because no catalyst was used for fabrication, the vapor−solid (VS) growth mechanism is proposed for In_2Se_3 microwires. We have performed a number of experiments in order to reduce the diameter of the wires by tuning experimental conditions and could only obtain the diameter of 1 μm.

Material characterization of the as grown In_2Se_3 microwires was conducted to determine the crystallographic phase and the results are presented in Figure 3. Figure 3a shows the TEM image of a single microwire, which shows the length in several micrometers. The inset of the figure presents the image at a 1 μm scale showing the smooth surface of the as grown wires.

The high resolution TEM (HRTEM) analysis (Figure 3b) reveals the expected hexagonal lattice fringes with a lattice spacing of 0.35 nm, consistent with the (110) plane in XRD spectrum highest intensity peak. The corresponding selected area electron diffraction (SAED) pattern is shown in Figure 3c. The SAED spot pattern confirms the hexagonal crystalline structure of high quality. All the directions of the planes are marked according to the d-spacing and angles as depicted from XRD spectrum analysis. The SAED pattern clearly demonstrates that the microwires are not mixed phase but in fact high crystalline in nature. There exists at least five different phases (α, β, γ, κ and δ) of stoichiometric In_2Se_3 with varying lattice parameters: α-phase, a = 4.02 Å, c = 19.23 Å;[36] β-phase, a = 4.01 Å, c = 19.22 Å;[37] γ-phase, a = 7.12 Å, c = 19.38 Å;[38] κ-phase, a = 8.09 Å, c = 19.85 Å;[39] δ-phase, a = 4.00 Å, c = 19.28 Å.[40] Although, discrepancies do exist in the literature. Figure 3d shows the XRD spectrum of as-synthesized In_2Se_3 microwires in furnace tube using elemental In and Se powders as precursors. Millar indices of every peak are indexed in the figure and it is observed that the main peaks located at 2θ = 24.94, 27.54, 37.46, 43.90 and 52.54° corresponding to the (110), (006), (116), (207) and (306) planes, respectively, have the highest intensity. All the peaks match well with the peaks of hexagonal In_2Se_3 except one peak present at 2θ = 21° which correspond to indium oxide. The slight extra amounts in indium powders present in the crucible might have been converted to indium oxide as the upper empty portion of the crucible contained air before placing in the furnace tube. Although the tube was heavily flushed with high purity Ar, still there might be a chance of air trapping. The lattice parameters calculated for hexagonal In_2Se_3 are a =7.1286 Å and c =19.3810 Å, which correspond to the standard values of JCPDS card No. 89-0658 for In_2Se_3. It is clearly evident from the crystallographic lattice parameters that the γ-phase evolves as a result of

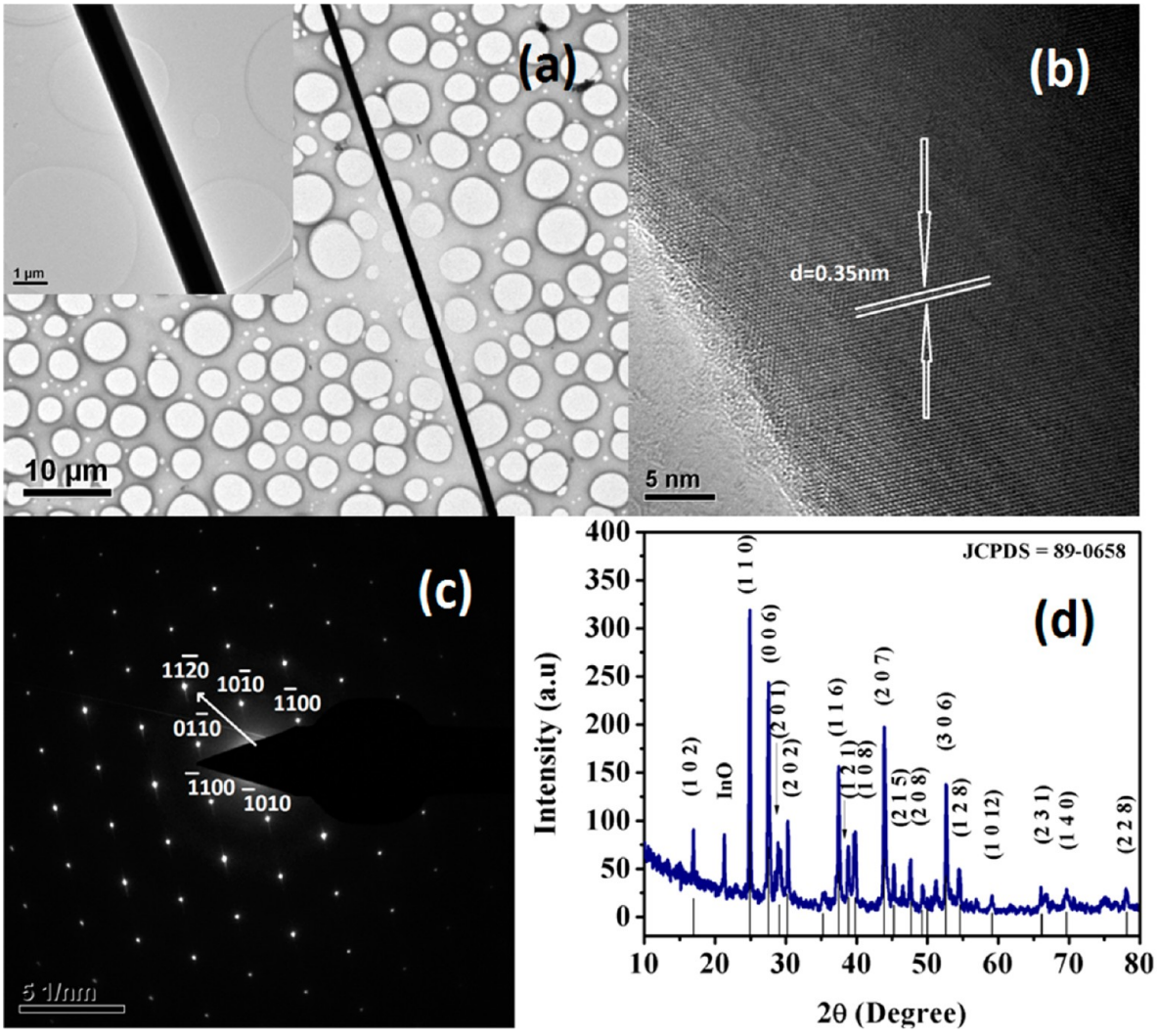

Figure 3. (a) TEM image of single In_2Se_3 microwire at a 10 μm scale showing length in several micrometers and inset shows the TEM image at a 1 μm scale showing the smooth surface of the wire. (b) HRTEM image of single microwire showing the d spacing. (c) Corresponding SAED pattern obtained from HRTEM image showing Hexagonal crystal structure with plane orientations. (d) Millar Indices marked XRD spectrum of the wires.

VS growth mechanism while the α-phase has been reported in literature[30−34] with a VLS growth mechanism, using Au as a catalyst for the nanowires' growth. Because properties of In_2Se_3 change with phase, so we have fabricated the photodetector with γ-phase In_2Se_3 prepared by a VS growth mechanism without using any catalyst.

In_2Se_3 microwires were further characterized by photoelectron spectroscopy (XPS) and the results are presented in Figure 4.

From the full scale survey spectrum (Figure 4a), it is evident that all the spectral features observed point toward the pure phase indium selenide. The In 3d5 and Se 3d doublets can be well-approximated by a combination of individual components that verify the unique chemical states of In and Se in In_2Se_3. The stoichiometric ratios of In and Se estimated by XPS analysis were 2:3, which confirmed the stoichiometric ratios depicted by energy dispersive x-ray spectroscopy (EDX) of a single wire presented in Figure 4d.

The electrical properties were measured using a traditional two probe method. Photodetector response under a laser (MellesGriot) with various wavelengths dependent intensities was measured and is presented in Figure 5. Figure 5a,b shows the typical I−V characteristics of the In_2Se_3 microwires photodetector measured under dark and illumination conditions with different wavelengths. Gold was used at the contacts in the photodetector. A little nonlinearity of the I−V curves is relative to the mismatch work function between In_2Se_3 microwires and gold. The current increases drastically under illumination as compared to the dark current. The measured values of dark and illuminated currents are on a nanoampere scale ∼1−10 nA, which are higher than any values reported for the given morphology (wires). These values are a direct function of the diameter of the wires, because our fabricated wires have a diameter of ∼1 μm, therefore the dark and light currents are expected to be higher. Both the dark and illuminated I−V curves pass through the origin, which demonstrates that there is no contribution of current generated by photovoltaic effect (zero short-circuit current). Under light illumination, the photodetector current increases drastically, particularly at high voltage bias shown as the red line in Figure 5a. The ratio of light current to dark current at a wavelength of 633 nm comes out to be 6.2.

Microwire photodetector response time was measured by a pulse generator controlled laser light. Figure 5c,d shows the

dx.doi.org/10.1021/am501933p | ACS Appl. Mater. Interfaces 2014, 6, 9550−9556

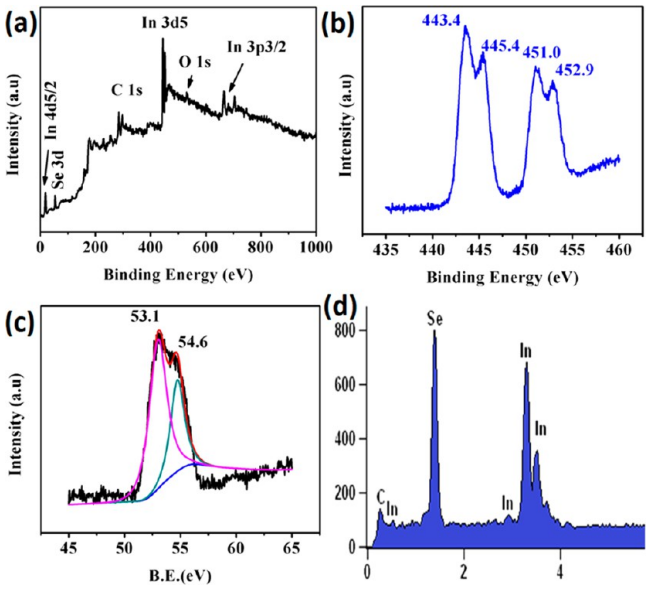

Figure 4. (a) Full scale XPS scan of the as-synthesized product in powder form. (b) Indium peaks in XPS spectra. (c) Se 3d doublets well-resolved in In_2Se_3 microwires. (d) EDX spectra acquired from a single microwire showing stoichiometric ratios of In and Se of 2:3.

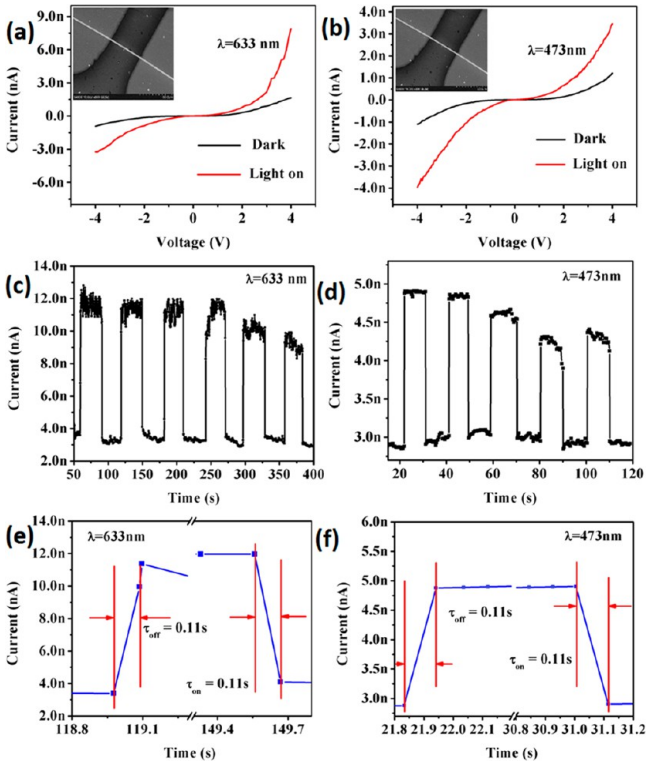

Figure 5. Photoresponse characteristics of device fabricated of a single In_2Se_3 microwire. (a,b) Typical I–V curves of the device under dark and light illuminated by a laser at 633 and 473 nm wavelengths, respectively; inset shows the single microwire with Au contacts. (c,d) Time dependent photoresponse of the device with laser on and off. (e,f) Single-cycle response characteristics of the photodetector for rise/fall time analysis.

transient current waveform in response to a series of cycles with alternating ON and OFF of the light source.

The In_2Se_3 microwire photodetector exhibits a repeatable and reasonably stable response to incident light. Figure 5e,f shows the single cycle response of light ON and OFF (by taking 0 to 100% photocurrent change for the rise times and 100 to 0% for the fall times) for 633 and 473 nm wavelengths, respectively. The measured rise and fall times were 0.11 s, demonstrating reasonable response performance for a resistor-mode photodetector and showing better results as compared to already reported results.[41]

The performance of the photodetector was further evaluated by measuring the two other key figures of merits (FOMs), namely responsivity (R_λ) and external quantum efficiency (EQE). The R_λ and EQE are key parameters that determine the sensitivity of the photodetector. R_λ is defined as the photocurrent generated per unit power of incident light on the effective area of the photodetector,[10] given as eq 1.

$$R_\lambda = \Delta I_\lambda/(P_\lambda A) \quad (1)$$

Here ΔI_λ is the photocurrent and is the difference of light and dark currents at a given biased voltage ($I_\lambda - I_{dark}$), P_λ is the intensity of the incident light and A is the effective illuminated surface area. The values of ΔI_λ for 633 and 473 nm wavelengths are 6.7 and 2.5 nA, respectively. P_λ is 6.2 mW/cm^2 for 633 nm and 5.5 mW/cm^2 for 473 nm wavelengths and the effective illuminated surface area is 2.05 μm^2 for both wavelengths. The responsivity of the photodetector for 633 and 473 nm wavelengths comes out to be 0.54 and 0.23A/W, respectively (at 4 V). The photodetector shows better performance as compared to the reported in literature.[42] The reason for such a sensitive photodetector is the high values of dark and light currents, which, in turn, is the result of a larger diameter, as discussed earlier.

External quantum efficiency (EQE) can be defined as the number of electrons detected per every incident photon[43] and can be calculated by relation 2.

$$EQE = hcR_\lambda/(e\lambda) \quad (2)$$

Here h is Planck's constant, c is velocity of light, e is electronic charge, and λ is incident light wavelength. The EQEs for wavelengths of 633 and 473 nm are 1.23 and 0.60, respectively (at 4 V).

The current response of the photodetector in various wavelength regions is shown in Figure 6. Figure 6a shows the current response in UV–vis spectrum at different wavelengths. The response of the photodetector is appreciable from UV–NIR spectrum. Figure 6b shows the response of the photodetector in the NIR region at different wavelengths. These two graphs indicate that the photodetector can detect light in a wide spectrum from the UV–NIR region. These wide range photodetectors have immense importance in next-generation electronics and devices. When the photodetector was exposed to a halogen lamp instead of a laser illumination source, it still shows significant response, indicating the wide range of applications of catalyst free grown In_2Se_3 microwire based photodetectors. We believe that this wide range, cost effective and simply fabricated photodetector will be a hot topic of research in future device fabrication technology. The photodetector response was further analyzed by calculating the specific detectivity, which is a key parameter and a performance indicator in photodetector fabrication technology, and the results are shown in Figure 6d.

The specific detectivity (D^*) is the characteristic detectivity (D) multiplied by the square root of the photodetector area

dx.doi.org/10.1021/am501933p | ACS Appl. Mater. Interfaces 2014, 6, 9550–9556

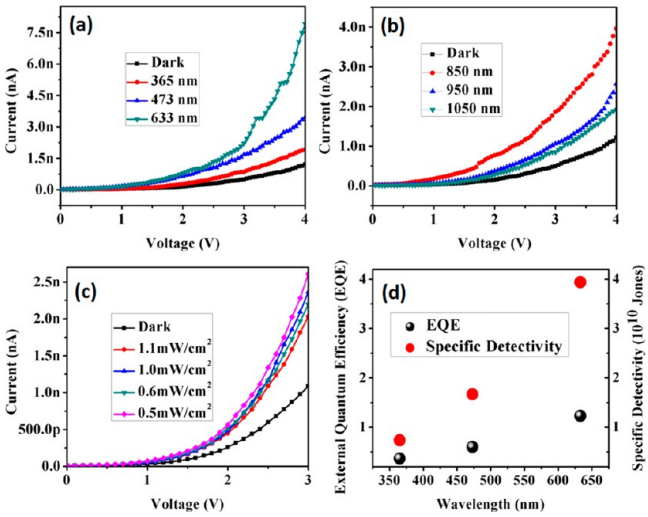

Figure 6. (a) Photoresponse of the photodetector at different wavelengths showing UV–vis range. (b) Photoresponse at NIR region. (c) Photoresponse at different intensities of halogen lamp. (d) EQE and specific detectivity curves showing the sensitivity of the detector.

(A) ($D^* = D\sqrt{A}$). Here D is the inverse of noise-equivalent power (NEP). The NEP, defined as the minimum input optical power to generate photocurrent equal to the RMS noise current in 1 Hz bandwidth,[44] is essentially the minimum detectable signal. The specific detectivity allows different systems to be compared independent of device area and band width. The specific detectivity (D^*) in the unit of Jones was calculated using $D^* = R_\lambda A^{1/2}/(2eI_{dark})^{1/2}$, where R_λ is the responsivity, A is the device effective area and I_{dark} is the dark current.[45] The specific detectivity (at 4 V) was calculated to be $\sim 3.94 \times 10^{10}$ Jones at 633 nm and 1.67×10^{10} Jones at 473 nm wavelengths, respectively. Figure 6d shows the EQE and specific detectivity at each wavelength under monochromatic illumination and demonstrates the reasonable response from catalyst free grown In_2Se_3 single microwire based photodetectors.

CONCLUSION

For the first time, we present the synthesis of high quality In_2Se_3 microwires by a vapor–solid approach without using any catalyst and demonstrate the photoconductive characteristics of an individual microwire. The high quality microwires are synthesized on a large scale and single crystalline in nature. The wires have a uniform diameter of ~ 1 μm and length of several micrometers. These ultralong wires have never been reported to date. The photodetector based on catalyst free grown microwires possess fast, reversible and stable photoresponse when exposed to different wavelengths of light. To investigate the performance of the photodetector, the key figure of merits were calculated. The photodetector exhibits a photoresponsivity of 0.54 A/W and an external quantum efficiency (EQE) of 1.23 at 633 nm with 4 V bias. The photodetector has a reasonable response time of 0.11 s and a specific detectivity of 3.94×10^{10} Jones at 633 nm with a light detection range from 350 to 1050 nm. The results indicate that the catalyst free growth mechanism for In_2Se_3 microwires with high quality and single-crystallographic phase has immense potential in future devices such as UV–vis-NIR detectors, biomedical imaging, high-resolution video recording, astronomy and photovoltaics.

AUTHOR INFORMATION

Corresponding Author

*Chuanbao Cao. E-mail: cbcao@bit.edu.cn. Tel: +86 10 68913792. Fax: +86 10 68912001.

Notes

The authors declare no competing financial interest.

ACKNOWLEDGMENTS

This work was supported by National Natural Science Foundation of China (21371023, 50972017) and the Research Fund for the Doctoral Program of Higher Education of China (20101101110026)

REFERENCES

(1) Fang, X. S.; Bando, Y.; Liao, M. Y.; Zhai, T. Y.; Gautam, U. K.; Li, L.; Koide, Y.; Golberg, D. An Efficient Way to Assemble ZnS Nanobelts as Ultraviolet-Light Sensors with Enhanced Photocurrent and Stability. *Adv. Funct. Mater.* **2010**, *20*, 500–508.

(2) Zhai, T. Y.; Fang, X. S.; Bando, Y.; Dierre, B.; Liu, B. D.; Zeng, H. B.; Huang, Y.; Xu, X. J.; Yuan, X. L.; Sekiguchi, T.; Golberg, D. Characterization, Cathodoluminescence, and Field-Emission Properties of Morphology-Tunable CdS Micro/Nanostructures. *Adv. Funct. Mater.* **2009**, *19*, 2423–30.

(3) Fang, X. S.; Xiong, S. L.; Zhai, T. Y.; Bando, Y.; Liao, M. Y.; Gautam, U. K.; Koide, Y.; Zhang, X. G.; Qian, Y. T.; Golberg, D. High-Performance Bule/Ultraviolet-Light-Sensitive ZnSe-Nanobelt Photodetectors. *Adv. Mater.* **2009**, *21*, 5016–5021.

(4) Pan, Z. W.; Dai, Z. R.; Wang, Z. L. Nanobelts of Semiconducting Oxides. *Science* **2001**, *291*, 1947–49.

(5) Zhai, T. Y.; Zhong, H. Z.; Gu, Z. J.; Peng, A. D.; Fu, H. B.; Ma, Y.; Li, Y. F.; Yao, J. N. Manipulation of the Morphology of ZnSe Submicron Structures Using CdSe Nanocrystals as the Seeds. *J. Phys. Chem. C* **2007**, *111*, 2980–86.

(6) Ye, C. H.; Fang, X. S.; Hao, Y. F.; Teng, X. M.; Zhang, L. D. Zinc Oxide Nanostructures: Morphology Derivation and Evolution. *J. Phys. Chem. B* **2005**, *109*, 19758–65.

(7) Ali, Z.; Cao, C. B.; Li, L. J.; Wang, Y. L.; Cao, T.; Tahir, M.; Idrees, F.; Butt, F. K. Effect of Synthesis Technique on Electrochemical Performance of Bismuth Selenide. *J. Power Sources* **2013**, *29*, 216–212.

(8) Ali, Z.; Cao, C. B.; Khan, W. S.; Butt, F. K.; Hussain, S.; Mahmood, T.; Nabi, G.; Usman, Z. Simultaneous Growth of ZnSe Cactus-Like Structures and Novel Microflowers of Selenium. *J. Alloys Compd.* **2012**, *513*, 620–625.

(9) Xuelian, Y.; Cao, C. B.; Zhu, H. S. Synthesis and Photoluminescence Properties of Bi_2S_3 Nanowires via Surfactant Micelle-Template Inducing Reaction. *Solid. State Commun.* **2005**, *134*, 239–243.

(10) Zhai, T. Y.; Fang, X. S.; Liao, M. Y.; Xu, X. J.; Li, L.; Liu, B. D.; Koide, Y.; Ma, Y.; Yao, J.; Bando, Y.; Golberg, D. Fabrication of High-Quality In_2Se_3 Nanowire Arrays toward High-Performance Visible-Light Photodetectors. *ACS Nano* **2010**, *4*, 1596–1602.

(11) Jie, J. S.; Zhang, W. J.; Jiang, Y.; Meng, X. M.; Li, Y. Q.; Lee, S. T. Photoconductive Characteristics of Single-Crystal CdS Nanoribbons. *Nano Lett.* **2006**, *6*, 1887–92.

(12) Lin, D. D.; Wu, H.; Pan, W. Photoswitches and Memories Assembled by Electrospinning Aluminum-Doped Zinc Oxide Single Nanowires. *Adv. Mater.* **2007**, *19*, 3968–72.

(13) Xuelian, Y.; Cao, C. B. Photoresponse and Field-Emission Properties of Bismuth Sulfide Nanoflowers. *Cryst. Growth Des.* **2008**, *8*, 3951–3955.

(14) Butt, F. K.; Mirza, M.; Cao, C.B.; Idrees, F.; Tahir, M.; Safdar, M.; Ali, Z.; Tanveer, M.; Aslam, I. Synthesis of Mid-Infrared SnSe Nanowires and their Optoelectronic Properties. *CrystEngComm* **2014**, *16*, 3470–3473.

(15) Jiang, Y.; Zhang, W. J.; Jie, J. S.; Meng, X. M.; Fan, X.; Lee, S. T. Photoresponse Properties of CdSe Single-Nanoribbon Photodetectors. *Adv. Funct. Mater.* **2007**, *17*, 1795−1800.
(16) Liao, M. Y.; Koide, Y.; Alvarez, J.; Imura, M.; Kleider, J. P. Persistent Positive and Transient Absolute Negative Phtoconductivity Observed in Diamond Photodetectors. *Phys. Rev. B* **2008**, *78*, 045112−19.
(17) Zhai, T. Y.; Fang, X. S.; Liao, M. Y.; Xu, X. J.; Zeng, H. B.; Bando, Y.; Golberg, D. Comprehensive Review of One-Dimensional Metal-Oxide Nanostructure Photodetectors. *Sensors* **2009**, *9*, 6504−29.
(18) Julien, C.; Hatzikraniotis, E.; Kambas, K. Electrical Transport-Properties of Impurity-Doped In2Se_3. *Phys. Status Solidi A* **1986**, *97*, 579−585.
(19) Shen, G. Z.; Chen, D.; Chen, P. C.; Zhou, C. W. Vapor-Solid Growth of One-Dimensional Layer-Structured Gallium Sulfide Nanostructures. *ACS Nano* **2009**, *3*, 1115−1120.
(20) Lyu, D. Y.; Lin, T. Y.; Lin, J. H.; Tseng, S. C.; Hwang, J. S.; Chiang, H. P.; Chiang, C. C.; Lan, S. M. Growth and Properties of Single-Phase γ-In_2Se_3 Thin Films on (111) Si Substrate by AP-MOCVD using H_2Se Precursor. *Sol. Energy Mater. Sol. Cells* **2007**, *91*, 888−92.
(21) Peng, H. L.; Schoen, D. T.; Meister, S.; Zheng, X. F.; Cui, Y. J. Synthesis and Phase Transformation of In_2Se_3 and $CuInSe_2$ Nanowires. *J. Am. Chem. Soc.* **2007**, *129*, 34−35.
(22) Vaidyanathan, R.; Stickney, J. L.; Cox, S. M.; Compton, S. P.; Happek, U. Formation of In_2Se_3 Thin Films and Nanostructures Using Electrochemical Atomic Layer Epitaxy. *J. Electroanal. Chem.* **2003**, *559*, 55−61.
(23) Lai, K. J.; Peng, H. L.; Kundhikanjana, W.; Schoen, D. T.; Xie, C.; Meister, S.; Cui, Y.; Kelly, M. A.; Shen, Z. X. Nanoscale Electronic Inhomogeneity in In_2Se_3 Nanoribbons Revealed by Microwave Impedance Microscopy. *Nano Lett.* **2009**, *9*, 1265−69.
(24) Peng, H. L.; Xie, C.; Schoen, D. T.; Cui, Y. Large Anisotropy of Electrical Properties in Layer-Structured In_2Se_3 Nanowires. *Nano Lett.* **2008**, *8*, 1511−16.
(25) Yu, B.; Ju, S.; Sun, X. H.; Ng, G.; Nguyen, T. D.; Meyyappan, M.; Janes, D. B. Indium Selenide Nanowire Phase-Charge Memory. *Appl. Phys. Lett.* **2007**, *91*, 133119−21.
(26) Chang, K. J.; Lahn, S. M.; Chang, J. Y. Growth of Single-Phase by Using Metal Organic Chemical Vapor Deposition with Dual-Source Precursors. *Appl. Phys. Lett.* **2006**, *89*, 182118−21.
(27) Cheon, J. W.; Arnold, J.; Yu, K. M.; Bourret, E. D. Metalorganic Chemical Vapor Deposition of Semiconducting III/VI In_2Se_3 Thin Films from the Single-Source Precursor: $In[SeC(SiMe_3)_3]_3$. *Chem. Mater.* **1995**, *7*, 2273−76.
(28) De Groot, C. H.; Moodera, J. S. Growth and Characterization of a Novel In2Se_3 Structure. *J. Appl. Phys.* **2001**, *89*, 4336−40.
(29) Stoll, S. L.; Barron, A. R. Metal-Organic Chemical Vapor Deposition of Indium Selenide (InSe) thin Films. *Chem. Mater.* **1998**, *10*, 650−57.
(30) Schoen, D. T.; Peng, H.; Cui, Y. Anisotropy of Chemical Transformation from In_2Se_3 to $CuInSe_2$ Nanowires through Solid State Reaction. *J. Am. Chem. Soc.* **2009**, *131*, 7973−7975.
(31) Mafi, E.; Soudi, A.; Gu, Y. Electronically Driven Amorphization in Phase-Change In_2Se_3 Nanowires. *J. Phys. Chem. C* **2012**, *116*, 22539−22544.
(32) Sun, X. H.; Yu, B.; Garrick, N. G.; Nguyen, T. D.; Meyyappan, M. III-VI Compound Semiconductor Indium Selenide (In_2Se_3) Nanowires: Synthesis and Characterization. *Appl. Phys. Lett.* **2006**, *89*, 233121−23.
(33) Baek, C. K.; Kang, D. G.; Kim, J. S.; Jin, B.; Rim, T.; Park, S. Y.; Meyyappan, M.; Jeong, Y. H.; Lee, J. S. Improved Performance of In_2Se_3 Nanowire Phase-Change Memory with SiO_2 Passivation. *Solid-State Electron.* **2013**, *80*, 10−13.
(34) Li, Y.; Gao, J.; Li, Q. L.; Peng, M. F.; Sun, X. H.; Li, Y. Y.; Yuan, G.; Wen, W.; Meyyappan, M. *J.* Thermal Phase Transformation of In_2Se_3Nanowires Studied by in situ Synchrotron Radiation X-ray Diffraction. *Mater. Chem.* **2011**, *21*, 6944−6947.
(35) Wang, J. J.; Cao, F. F.; Jiang, L.; Guo, Y. G.; Hu, W. P.; Wan, L. J. High Performance Photodetectors of Individual InSe Single Crystalline Nanowire. *J. Am. Chem. Soc.* **2009**, *131*, 15602−15603.
(36) Popovic, S.; Tonejc, A.; Grzeta-Plenkovic, B.; Celustka, B.; Trojko, R. Revised and New Crystal Data for Indium Selenides. *J. Appl. Crystallogr.* **1979**, *12*, 416−420.
(37) Lutz, H.; Fischer, M.; Baldus, H.-P.; Blachnik, R. Zur Polymorphie des In_2Se_3. *J. Less-Common Met.* **1988**, *143*, 83−92.
(38) Pfitzner, A.; Lutz, H. D. Redetermination of the Crystal Structure of Gamma-In_2Se_3 by Twin Crystal X-Ray Method. *J. Solid State Chem.* **1996**, *124*, 305−308.
(39) Jasinski, J.; Swider, W.; Washburn, J.; Liliental-Weber, Z.; Chaiken, A.; Nauka, K.; Gibson, G. A.; Yang, C. C. Crystal Structure of k-In_2Se_3. *Appl. Phys. Lett.* **2002**, *81*, 4356−4358.
(40) Drapak, S. I.; Kovalyuk, Z. D. Asymmetric Current Flow in a Native Oxide/Indium Selenide Heterostructure. *Inorg. Mater.* **2011**, *47*, 1178−1182.
(41) Zhai, T. Y.; Ma, Y.; Li, L.; Fang, X. S.; Liao, M. Y.; Koide, Y.; Yao, J. N.; Bando, Y.; Goldberg, D. Morphology-tunable In_2Se_3Nanostructures with Enhanced Electrical and Photoelectrical Performances via Sulfur Doping. *Mater. Chem.* **2010**, *20*, 6630−6637.
(42) Zhai, T. Y.; Fang, X. S.; Liao, M. Y.; Xu, X. J.; Li, L.; Liu, B. D.; Koide, Y.; Ma, Y.; Yao, J. N.; Bando, Y.; Golberg, D. Fabrication of High-Quality In_2Se_3Nanowire Arrays Towards High-Performance Visible-Light Photodetectors. *ACS Nano* **2010**, *4*, 1596−1602.
(43) Wang, Z. X.; Safdar, M.; Jiang, C.; He, J. High-Performance UV Visible NIR Broad Spectral Photodetectors Based on One-Dimensional In_2Te_3 Nanostructures. *Nano Lett.* **2012**, *12*, 4715−4721.
(44) Li, Q. L.; Li, Y.; Gao, J.; Wang, S. D.; Sun, X. H. High Performance Single In_2Se_3Nanowire Photodetector. *Appl. Phys. Lett.* **2011**, *99*, 243105−08.
(45) Hu, P.; Wang, L.; Yoon, M.; Zhang, J.; Feng, W.; Wang, X.; Wen, Z.; Idrobo, J. C.; Miyamoto, Y.; Geohegan, D. B. Highly Responsive Ultrathin GaS Nanosheet Photodetectors on Rigid and Flexible Substrates. *Nano Lett.* **2013**, *13*, 1649−1654.